

# Preliminary Examination

Tianchen (Gary) Hu

Department of Mechanical Engineering & Materials Science  
Pratt School of Engineering  
Duke University

Exam Committee:      John Dolbow  
                          Wilkins Aquino  
                          Johann Guilleminot  
                          Manolis Vafeakis  
                          Benjamin Spencer

1:00 pm – 3:00 pm EDT  
April 2nd, 2020

# Overview

---

## For the Committee

- Courses taken
- Courses TA'd
- RCR trainings

## Past work

- Theory
- Soil Desiccation
- Intergranular Fracture in UO<sub>2</sub>

## Future work

- Proposal
- Timeline

## Preliminary results and findings

- Towards ductile fracture
- Incorporating thermal effects

## References

Course number	Course title	Grade
MATH 551	Applied Partial Differential Equation & Complex Variables	A
ME 524	Finite Element Method	A
CEE 531	Finite Elements for Fluids	A
CEE 690	Uncertainty Quantification	A
ECE 551D	Programming, Data Structures & Algorithms in C++	A
CEE 521	Elasticity	A
MATH 561	Numerical Linear Algebra	A
MATH 731	Advanced Calculus I	A-
CEE 630	Nonlinear Finite Element Analysis	A+
ME 555	Numerical Methods for Nonlinear Optimization	A+
CEE 520	Continuum Mechanics	
CEE 690	Multiscale Methods	

See [unofficial\\_transcript.pdf](#) for details.

Semester	Course number	Course title	Instructor
Fall 2018	CEE 530	Finite Element Method	Wilkins Aquino
Fall 2019	CEE 530	Finite Element Method	Wilkins Aquino

Training topic	Credit
The Graduate School RCR Orientation	6.0
Introduction to Archives and Repositories	2.0
Text Recycling & Self-plagiarism	3.0
Research Data Management 101 for Scientists	2.0
	13.0

See [unofficial\\_transcript.pdf](#) for details.

For the Committee

Courses taken

Courses TA'd

RCR trainings

**Past work**

Theory

Soil Desiccation

Intergranular Fracture in UO<sub>2</sub>

Future work

Proposal

Timeline

Preliminary results and findings

Towards ductile fracture

Incorporating thermal effects

References

For the Committee

Courses taken

Courses TA'd

RCR trainings

**Past work**

Theory

Soil Desiccation

Intergranular Fracture in UO<sub>2</sub>

Future work

Proposal

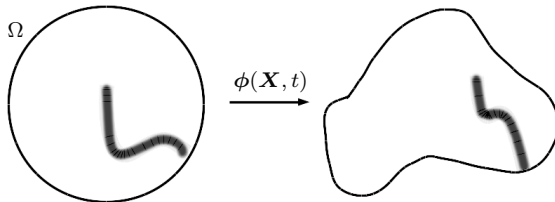
Timeline

Preliminary results and findings

Towards ductile fracture

Incorporating thermal effects

References

**Kinematics**

$X$ : material point

$x$ : spatial point

$\Omega$ : reference configuration

$\partial\Omega$ : external boundary

$\Gamma$ : permanent crack set

$\phi(X, t)$ : deformation map

$F = \partial x / \partial X$ : deformation gradient

$J = \det(F)$ : jacobian

**Observable quantities**

$T$ : temperature

$F$ : deformation gradient

**State**

$S = \{T, F\}$

$\mathcal{X} = \{F^p, \bar{\varepsilon}^p, d, \nabla d\}$

$\pi = \rho_0 \psi$ : Helmholtz free energy

**Internal variables**

$F^p$ : plastic deformation gradient

$\bar{\varepsilon}^p$ : effective uniaxial plastic strain

$d, \nabla d$ : phase-field

### Balance laws

Mass balance (no mass transport):

$$J\rho = \rho_0 \quad (1)$$

Linear momentum balance:

$$\nabla \cdot \mathbf{P} + \rho_0 \mathbf{b} = \mathbf{0} \quad (2)$$

Angular momentum balance:

$$\mathbf{P}\mathbf{F}^T = \mathbf{F}\mathbf{P}^T \quad (3)$$

Energy balance (1st law, adiabatic):

$$\mathbf{P} : \dot{\mathbf{F}} + \rho_0 r = \dot{\pi} + \rho_0 T \dot{s} + \rho_0 \dot{T} s \quad (4)$$

$$\rho_0 c \dot{T} = \rho_0 r - \pi_{,\bar{\varepsilon}^p} \dot{\bar{\varepsilon}}^p - \pi_{,d} \dot{d} \quad (5)$$

Entropy production (2nd law, or Clausius-Duhem inequality):

$$-\dot{\pi} - \rho_0 s \dot{T} + \mathbf{P} : \dot{\mathbf{F}} \geq 0 \quad (6)$$

## Constitutive constraints

The specific entropy:

$$s = -\psi_{,T} \quad (7)$$

The first Piola-Kirchhoff stress:

$$\boldsymbol{P} = \pi_{,\boldsymbol{F}} \quad (8)$$

The dissipation inequality:

$$-\pi_{,\boldsymbol{F}^p} : \dot{\boldsymbol{F}}^p - \pi_{,\bar{\varepsilon}^p} \dot{\bar{\varepsilon}}^p - \pi_{,d} \dot{d} - \pi_{,\nabla d} \cdot \nabla \dot{d} \geq 0, \quad (9)$$

which, by the principle of maximum dissipation, gives me the equations of flow rule, yield surface and fracture evolution.

See [plasticity.pdf](#) for a detailed derivation of balance laws and constitutive equations.

In the soil desiccation problem, the free energy is written as

$$\pi = \pi_{\text{elastic}} + \pi_{\text{inelastic}} + \pi_{\text{interface}} + \pi_{\text{fracture}}. \quad (10)$$

In the UO<sub>2</sub> fracture problem, the free energy is written as

$$\pi = \begin{cases} \pi_{\text{elastic}}^{\text{bnd}} + \pi_{\text{fracture}}^{\text{bnd}}, & \forall \mathbf{X} \in \Omega^{\text{bnd}}, \\ \pi_{\text{elastic}}^{\text{grain}} + \pi_{\text{fracture}}^{\text{grain}}, & \forall \mathbf{X} \in \Omega^{\text{grain}}. \end{cases} \quad (11)$$

In the ductile fracture model, the free energy takes the following form:

$$\pi = \pi_{\text{elastic}} + \pi_{\text{plastic}} + \pi_{\text{fracture}}. \quad (12)$$

The free energy  $\pi$  is polyconvex and coercive. We adopt an alternating minimization technique to address stability issues (see e.g. [1] for a convergence proof).

See [algorithm.pdf](#) for the solution procedure.

Variational phase-field models (as a subclass of the gradient-damage models) rely on a relatively unified description of the fracture energy:

$$\pi_{\text{fracture}} = \mathcal{G}_c \gamma(d; l), \quad (13)$$

$$\gamma(d; l) = \frac{1}{c_0 l} [w(d) + 2l^2 \nabla d \cdot \nabla d], \quad (14)$$

where  $c_0$  is a normalization constant such that  $\lim_{l \searrow 0} \gamma(d; l) = \delta(\Gamma)$ .

### Cohesive fracture

$$w_1(d) = d,$$

$$g_{ql}(d) = \frac{1-d}{(1-d)+md}, \quad m = \frac{\mathcal{G}_c}{\pi_c} \frac{1}{c_0 l},$$

$$g_{qq}(d; p) = \frac{(1-d)^2}{(1-d)^2 + md(1+pd)}, \quad m = \frac{\mathcal{G}_c}{\pi_c} \frac{1}{c_0 l} \geq p+2.$$

### Brittle fracture

$$w_2(d) = d^2,$$

$$g_q(d) = (1-d)^2.$$

See [cohesive.pdf](#) for details in the cohesive fracture model.

For the Committee

Courses taken

Courses TA'd

RCR trainings

**Past work**

Theory

**Soil Desiccation**

Intergranular Fracture in UO<sub>2</sub>

Future work

Proposal

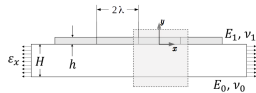
Timeline

Preliminary results and findings

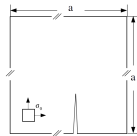
Towards ductile fracture

Incorporating thermal effects

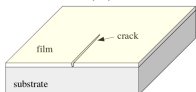
References



(a)



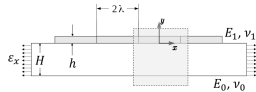
(b)



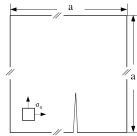
(c)

- ▶ Only “channeling” cracks in the thin film are considered.
- ▶ Small deformation is assumed for  $\pi_{\text{elastic}}$ , and  $\boldsymbol{\varepsilon} = (\nabla \mathbf{u} + \nabla^T \mathbf{u})/2$ .
- ▶ A frictionless contact split of the elastic energy is applied at the vicinity of the crack set.
- ▶ Thermal effects are neglected. Dehydration is modeled as pre-stress in  $\pi_{\text{inelastic}} = \sigma_0 \text{tr}(\boldsymbol{\varepsilon})$ .
- ▶ A cohesive-type fracture model is used for  $\pi_{\text{fracture}}$ .

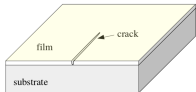
See mud.pdf for details.



(a)



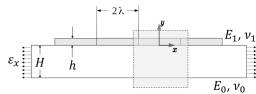
(b)



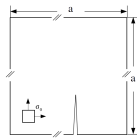
(c)

- ▶ Only “channeling” cracks in the thin film are considered.
- ▶ Small deformation is assumed for  $\pi_{\text{elastic}}$ , and  $\boldsymbol{\varepsilon} = (\nabla \mathbf{u} + \nabla^T \mathbf{u})/2$ .
- ▶ A frictionless contact split of the elastic energy is applied at the vicinity of the crack set.
- ▶ Thermal effects are neglected. Dehydration is modeled as pre-stress in  $\pi_{\text{inelastic}} = \sigma_0 \text{tr}(\boldsymbol{\varepsilon})$ .
- ▶ A cohesive-type fracture model is used for  $\pi_{\text{fracture}}$ .
- ▶ The model is verified with analytical solutions in a periodic quasi-1D context (Fig. a).

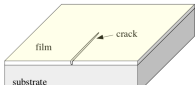
See mud.pdf for details.



(a)



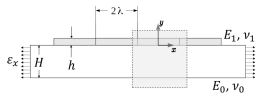
(b)



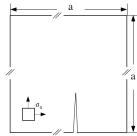
(c)

- ▶ Only “channeling” cracks in the thin film are considered.
- ▶ Small deformation is assumed for  $\pi_{\text{elastic}}$ , and  $\boldsymbol{\varepsilon} = (\nabla \mathbf{u} + \nabla^T \mathbf{u})/2$ .
- ▶ A frictionless contact split of the elastic energy is applied at the vicinity of the crack set.
- ▶ Thermal effects are neglected. Dehydration is modeled as pre-stress in  $\pi_{\text{inelastic}} = \sigma_0 \text{tr}(\boldsymbol{\varepsilon})$ .
- ▶ A cohesive-type fracture model is used for  $\pi_{\text{fracture}}$ .
- ▶ The model is verified with analytical solutions in a periodic quasi-1D context (Fig. a).
- ▶ Pervasive fracture is studied with a 2D simplification (Fig. b).
- ▶ The energy  $\pi_{\text{interface}}$  accounts for mismatch between the film and the substrate.
- ▶ Material property inhomogeneity in the macroscopic continuum model is taken into account by introducing two pointwise correlated random fields  $\{\mathcal{G}_c(\mathbf{X}), \mathbf{X} \in \Omega\}$  and  $\{\pi_c(\mathbf{X}), \mathbf{X} \in \Omega\}$ .

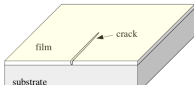
See mud.pdf for details.



(a)



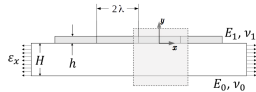
(b)



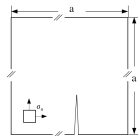
(c)

See [mud.pdf](#) for details.

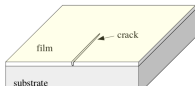
- ▶ Only “channeling” cracks in the thin film are considered.
- ▶ Small deformation is assumed for  $\pi_{\text{elastic}}$ , and  $\boldsymbol{\varepsilon} = (\nabla \mathbf{u} + \nabla^T \mathbf{u})/2$ .
- ▶ A frictionless contact split of the elastic energy is applied at the vicinity of the crack set.
- ▶ Thermal effects are neglected. Dehydration is modeled as pre-stress in  $\pi_{\text{inelastic}} = \sigma_0 \text{tr}(\boldsymbol{\varepsilon})$ .
- ▶ A cohesive-type fracture model is used for  $\pi_{\text{fracture}}$ .
- ▶ The model is verified with analytical solutions in a periodic quasi-1D context (Fig. a).
- ▶ Pervasive fracture is studied with a 2D simplification (Fig. b).
- ▶ The energy  $\pi_{\text{interface}}$  accounts for mismatch between the film and the substrate.
- ▶ Material property inhomogeneity in the macroscopic continuum model is taken into account by introducing two pointwise correlated random fields  $\{\mathcal{G}_c(\mathbf{X}), \mathbf{X} \in \Omega\}$  and  $\{\pi_c(\mathbf{X}), \mathbf{X} \in \Omega\}$ .
- ▶ The versatility offered by the probabilistic framework is highlighted by solving a 3D problem based on physical experiments.



(a)



(b)



(c)

- ▶ Only “channeling” cracks in the thin film are considered.
- ▶ Small deformation is assumed for  $\pi_{\text{elastic}}$ , and  $\boldsymbol{\varepsilon} = (\nabla \mathbf{u} + \nabla^T \mathbf{u})/2$ .
- ▶ A frictionless contact split of the elastic energy is applied at the vicinity of the crack set.
- ▶ Thermal effects are neglected. Dehydration is modeled as pre-stress in  $\pi_{\text{inelastic}} = \sigma_0 \text{tr}(\boldsymbol{\varepsilon})$ .
- ▶ A cohesive-type fracture model is used for  $\pi_{\text{fracture}}$ .
- ▶ The model is verified with analytical solutions in a periodic quasi-1D context (Fig. a).
- ▶ Pervasive fracture is studied with a 2D simplification (Fig. b).
- ▶ The energy  $\pi_{\text{interface}}$  accounts for mismatch between the film and the substrate.
- ▶ Material property inhomogeneity in the macroscopic continuum model is taken into account by introducing two pointwise correlated random fields  $\{\mathcal{G}_c(\mathbf{X}), \mathbf{X} \in \Omega\}$  and  $\{\pi_c(\mathbf{X}), \mathbf{X} \in \Omega\}$ .
- ▶ The versatility offered by the probabilistic framework is highlighted by solving a 3D problem based on physical experiments.

See [mud.pdf](#) for details.

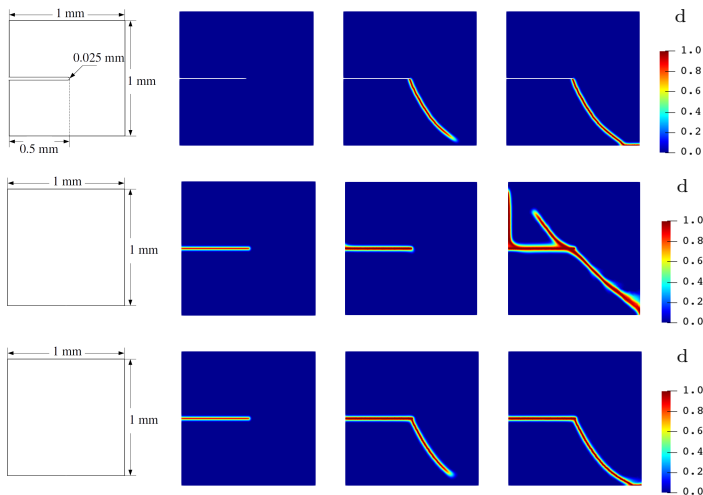
### The contact split

The elastic energy takes into account the tension-compression asymmetry and the frictionless contact condition at the vicinity of the crack set:

$$\pi_{\text{elastic}} = g_{qq}(d; p)\pi_{\text{elastic}}^{\langle A \rangle} + \pi_{\text{elastic}}^{\langle I \rangle}, \quad (15a)$$

$$\pi_{\text{elastic}}^{\langle A \rangle} = \begin{cases} \frac{1}{2}\lambda_s \langle \text{tr}(\boldsymbol{\varepsilon}) \rangle_+^2 + \mu_s \boldsymbol{\varepsilon}^+ : \boldsymbol{\varepsilon}^+, & d \leq d_{\text{critical}}, \\ \frac{1}{2}(\boldsymbol{\sigma}_n^+ + \boldsymbol{\sigma}_t) : \boldsymbol{\varepsilon}, & d > d_{\text{critical}}, \end{cases} \quad (15b)$$

$$\pi_{\text{elastic}}^{\langle I \rangle} = \begin{cases} \frac{1}{2}\lambda_s \langle \text{tr}(\boldsymbol{\varepsilon}) \rangle_-^2 + \mu_s \boldsymbol{\varepsilon}^- : \boldsymbol{\varepsilon}^-, & d \leq d_{\text{critical}}, \\ \frac{1}{2}\boldsymbol{\sigma}_n^- : \boldsymbol{\varepsilon}, & d > d_{\text{critical}}, \end{cases} \quad (15c)$$



The crack paths obtained using (1st row) the spectral decomposition on a geometrically notched plate, (2nd row) the spectral decomposition with an initial damage field, (3rd row) the contact split with an initial damage field.

Snapshots of crack paths are shown at (2nd column)  $u_x = 0 \text{ mm}$ , (3rd column)  $u_x = 0.0109 \text{ mm}$ , (4th column)  $u_x = 0.02 \text{ mm}$ .

### Material inhomogeneity

The covariance function  $\tau \mapsto R(\tau)$  for a  $[0, L]^n$   $p$ -periodic domain is given by

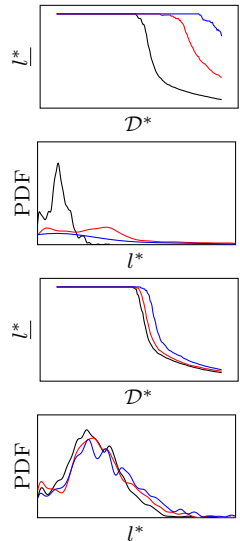
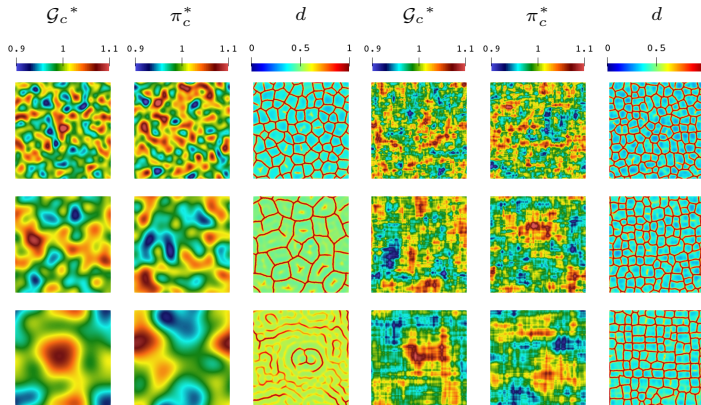
$$R(\tau) = \begin{bmatrix} R_1(\tau) & \rho R_1(\tau) \\ \rho R_1(\tau) & \rho^2 R_1(\tau) + (1 - \rho^2) R_2(\tau) \end{bmatrix}, \quad \forall \tau \in [0, p], \rho \in [-1, 1], \quad (16)$$

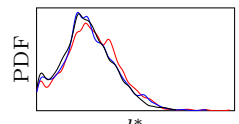
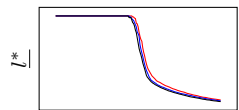
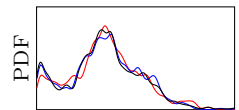
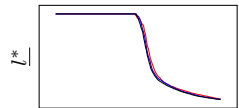
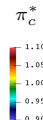
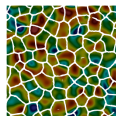
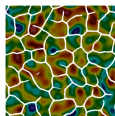
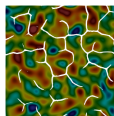
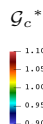
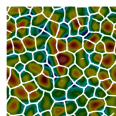
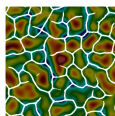
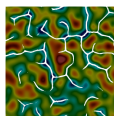
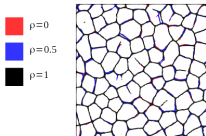
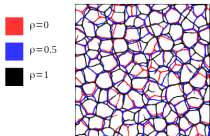
where the univariate covariance function  $R$  is assumed to take the generic form

$$R_\phi(\tau; L) = \exp(-c\phi(\tau; L)), \quad \forall \tau \in [0, p]. \quad (17)$$

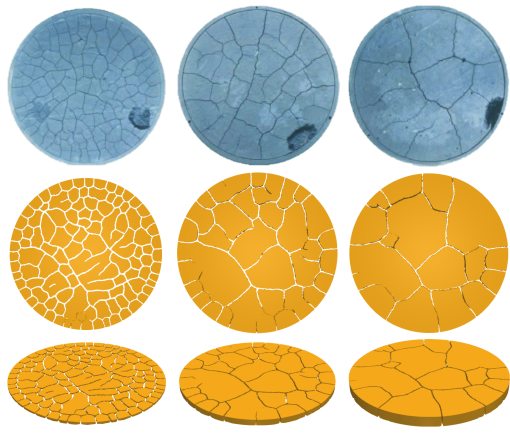
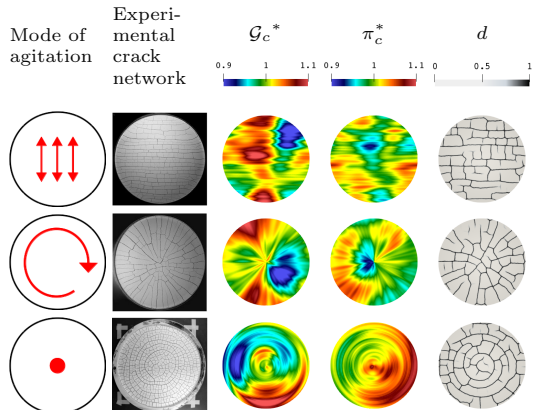
$\phi$  is a  $p$ -periodic function taken as

$$\phi(\tau; L) = \begin{cases} \frac{|\sin(\pi\tau/p)|}{L}, & (\text{Periodic Exponential, PE}), \\ \frac{\sin(\pi\tau/p)^2}{L^2}, & (\text{Periodic Squared-Exponential, PSE}). \end{cases} \quad (18)$$

Sensitivity to the correlation length  $L$ 

Sensitivity to  $\mathcal{G}_c$  and  $\pi_c$ 

### Flexibility of the stochastic model



For the Committee

Courses taken

Courses TA'd

RCR trainings

**Past work**

Theory

Soil Desiccation

Intergranular Fracture in UO<sub>2</sub>

Future work

Proposal

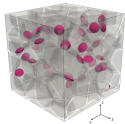
Timeline

Preliminary results and findings

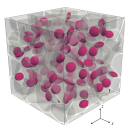
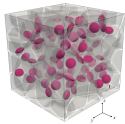
Towards ductile fracture

Incorporating thermal effects

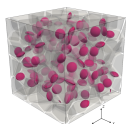
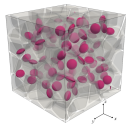
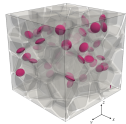
References



- ▶ A set of random close-packing (RCP) voronoi structures are realized by Maximal Poisson-disk Sampling (MPS).
- ▶ The polycrystalline microstructure is described by a set of non-conserved order variables  $\{\phi_i\}$  in a diffuse manner.
- ▶ The microstructure follows from a phase-field grain growth model [2].
- ▶ The grain boundaries are identified by  $\sum_i \phi_i^2 \geq 0.75$ .
- ▶ Gas bubbles are represented by another phase variable  $\phi_0$  and are uniformly distributed along grain boundaries, overriding existing order variables. The effect of gas pressure inside bubbles is neglected.

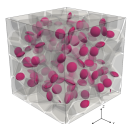
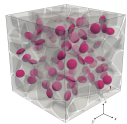
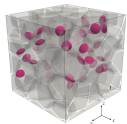


See [intergranular.pdf](#) for details.



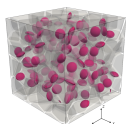
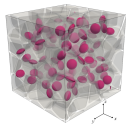
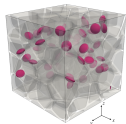
- ▶ A set of random close-packing (RCP) voronoi structures are realized by Maximal Poisson-disk Sampling (MPS).
- ▶ The polycrystalline microstructure is described by a set of non-conserved order variables  $\{\phi_i\}$  in a diffuse manner.
- ▶ The microstructure follows from a phase-field grain growth model [2].
- ▶ The grain boundaries are identified by  $\sum_i \phi_i^2 \geq 0.75$ .
- ▶ Gas bubbles are represented by another phase variable  $\phi_0$  and are uniformly distributed along grain boundaries, overriding existing order variables. The effect of gas pressure inside bubbles is neglected.
- ▶ A phase-field brittle fracture model is used.
- ▶ Grain boundaries have an arbitrarily high fracture toughness to facilitate intergranular fracture, i.e.  $\mathcal{G}_c^{\text{bnd}} \gg \mathcal{G}_c^{\text{grain}}$ .

See [intergranular.pdf](#) for details.



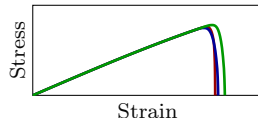
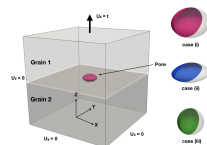
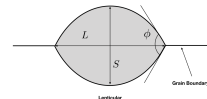
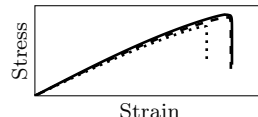
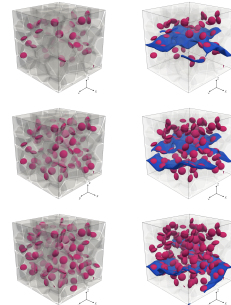
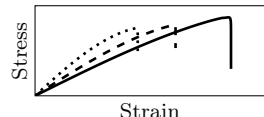
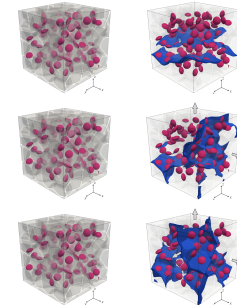
- ▶ A set of random close-packing (RCP) voronoi structures are realized by Maximal Poisson-disk Sampling (MPS).
- ▶ The polycrystalline microstructure is described by a set of non-conserved order variables  $\{\phi_i\}$  in a diffuse manner.
- ▶ The microstructure follows from a phase-field grain growth model [2].
- ▶ The grain boundaries are identified by  $\sum_i \phi_i^2 \geq 0.75$ .
- ▶ Gas bubbles are represented by another phase variable  $\phi_0$  and are uniformly distributed along grain boundaries, overriding existing order variables. The effect of gas pressure inside bubbles is neglected.
- ▶ A phase-field brittle fracture model is used.
- ▶ Grain boundaries have an arbitrarily high fracture toughness to facilitate intergranular fracture, i.e.  $\mathcal{G}_c^{\text{bnd}} \gg \mathcal{G}_c^{\text{grain}}$ .
- ▶ Numerical studies are performed to investigate the effect of bubble geometry, porosity and loading conditions on the fracture strength.

See [intergranular.pdf](#) for details.



- ▶ A set of random close-packing (RCP) voronoi structures are realized by Maximal Poisson-disk Sampling (MPS).
- ▶ The polycrystalline microstructure is described by a set of non-conserved order variables  $\{\phi_i\}$  in a diffuse manner.
- ▶ The microstructure follows from a phase-field grain growth model [2].
- ▶ The grain boundaries are identified by  $\sum_i \phi_i^2 \geq 0.75$ .
- ▶ Gas bubbles are represented by another phase variable  $\phi_0$  and are uniformly distributed along grain boundaries, overriding existing order variables. The effect of gas pressure inside bubbles is neglected.
- ▶ A phase-field brittle fracture model is used.
- ▶ Grain boundaries have an arbitrarily high fracture toughness to facilitate intergranular fracture, i.e.  $\mathcal{G}_c^{\text{bnd}} \gg \mathcal{G}_c^{\text{grain}}$ .
- ▶ Numerical studies are performed to investigate the effect of bubble geometry, porosity and loading conditions on the fracture strength.

See [intergranular.pdf](#) for details.

**Effect of bubble geometry****Effect of porosity****Effect of loading direction**

For the Committee

Courses taken

Courses TA'd

RCR trainings

Past work

Theory

Soil Desiccation

Intergranular Fracture in UO<sub>2</sub>

**Future work**

Proposal

Timeline

Preliminary results and findings

Towards ductile fracture

Incorporating thermal effects

References

**Challenge:** To predict material behavior with the presence of pervasive fracture. Cracks may nucleate, propagate, branch, and coalesce.

**Challenge:** To predict material behavior with the presence of pervasive fracture. Cracks may nucleate, propagate, branch, and coalesce.

**Techniques:** Element deletion, cohesive element insertion, mesh fragmentation, enrichment methods (XFEM, GFEM, etc.), damage models (local damage, gradient damage, phase-field), and counting...

**Challenge:** To predict material behavior with the presence of pervasive fracture. Cracks may nucleate, propagate, branch, and coalesce.

**Techniques:** Element deletion, cohesive element insertion, mesh fragmentation, enrichment methods (XFEM, GFEM, etc.), damage models (local damage, gradient damage, phase-field), and counting...

### **Current state of phase-field methods**

Elastic-fracture coupling: [3, 4, 5, 6, 7, 8, 9, 10].

Hyperelastic-fracture coupling concerning tension-compression asymmetry: [11, 12].

Tight Thermal-fracture coupling: [13, 14].

Plastic-fracture coupling: [15, 16, 17, 18, 19, 20].

Hyperelastic-plastic-thermal-fracture coupling: [13]

**Challenge:** To predict material behavior with the presence of pervasive fracture. Cracks may nucleate, propagate, branch, and coalesce.

**Techniques:** Element deletion, cohesive element insertion, mesh fragmentation, enrichment methods (XFEM, GFEM, etc.), damage models (local damage, gradient damage, phase-field), and counting...

### **Current state of phase-field methods**

Elastic-fracture coupling: [3, 4, 5, 6, 7, 8, 9, 10].

Hyperelastic-fracture coupling concerning tension-compression asymmetry: [11, 12].

Tight Thermal-fracture coupling: [13, 14].

Plastic-fracture coupling: [15, 16, 17, 18, 19, 20].

Hyperelastic-plastic-thermal-fracture coupling: [13]

**Is it good enough?** Sandia Fracture Challenge since 2012. Variational fracture models are not always the winner. Why...

**Challenge:** To predict material behavior with the presence of pervasive fracture. Cracks may nucleate, propagate, branch, and coalesce.

**Techniques:** Element deletion, cohesive element insertion, mesh fragmentation, enrichment methods (XFEM, GFEM, etc.), damage models (local damage, gradient damage, phase-field), and counting...

### **Current state of phase-field methods**

Elastic-fracture coupling: [3, 4, 5, 6, 7, 8, 9, 10].

Hyperelastic-fracture coupling concerning tension-compression asymmetry: [11, 12].

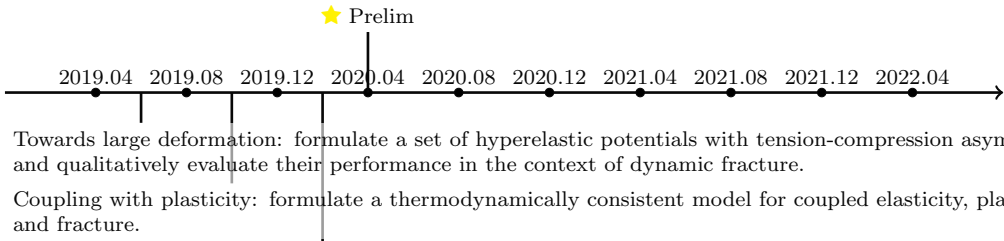
Tight Thermal-fracture coupling: [13, 14].

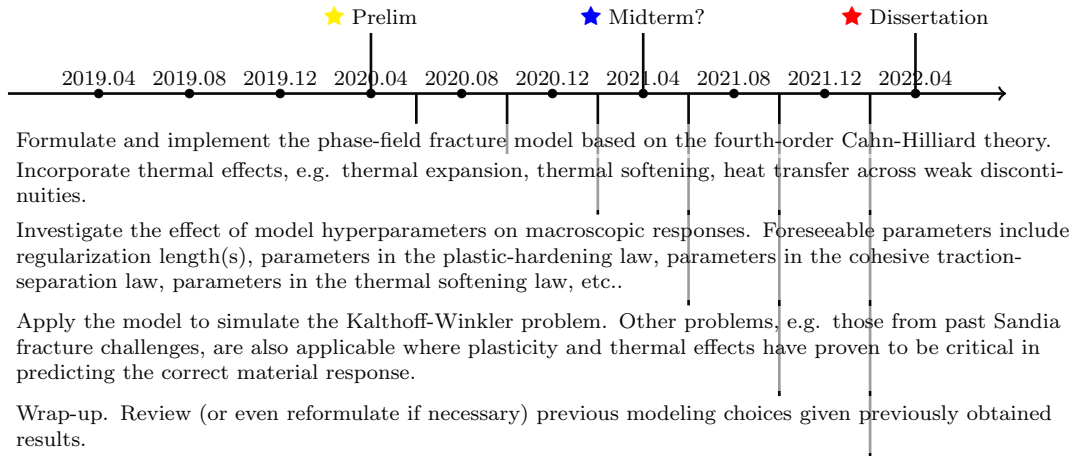
Plastic-fracture coupling: [15, 16, 17, 18, 19, 20].

Hyperelastic-plastic-thermal-fracture coupling: [13]

**Is it good enough?** Sandia Fracture Challenge since 2012. Variational fracture models are not always the winner. Why...

**Objective:** I propose to extend the state-of-the-art phase-field models to simulate large deformation ductile fracture with thermal effects under dynamic loading.





For the Committee

Courses taken

Courses TA'd

RCR trainings

Past work

Theory

Soil Desiccation

Intergranular Fracture in UO<sub>2</sub>

Future work

Proposal

Timeline

Preliminary results and findings

Towards ductile fracture

Incorporating thermal effects

References

For the Committee

Courses taken

Courses TA'd

RCR trainings

Past work

Theory

Soil Desiccation

Intergranular Fracture in UO<sub>2</sub>

Future work

Proposal

Timeline

**Preliminary results and findings**

Towards ductile fracture

Incorporating thermal effects

References

The free energy takes the following form

$$\pi(\mathbf{F}, \mathbf{F}^p, \bar{\varepsilon}^p, d, \nabla d) = \pi_{\text{elastic}}(\mathbf{F}, \mathbf{F}^p, d) + \pi_{\text{plastic}}(\bar{\varepsilon}^p, d) + \pi_{\text{fracture}}(d, \nabla d). \quad (19)$$

The elastic energy is defined as

$$\pi_{\text{elastic}}(\mathbf{F}, \mathbf{F}^p, d) = g^e(d) \pi_{\text{elastic}}^{(A)}(\mathbf{F}, \mathbf{F}^p) + \pi_{\text{elastic}}^{(I)}(\mathbf{F}), \quad (20a)$$

$$\pi_{\text{elastic}}^{(A)}(\mathbf{F}, \mathbf{F}^p) = H(J - 1) \left[ \frac{1}{2} K_s \left( \frac{1}{2}(J^2 - 1) - \ln J \right) \right] + \frac{1}{2} \mu_s (\bar{\mathbf{C}} : \mathbf{C}^{p-1} - 3), \quad (20b)$$

$$\pi_{\text{elastic}}^{(I)}(\mathbf{F}) = H(1 - J) \left[ \frac{1}{2} K_s \left( \frac{1}{2}(J^2 - 1) - \ln J \right) \right]. \quad (20c)$$

The plastic energy is defined as

$$\pi_{\text{plastic}}(\bar{\varepsilon}^p) = g^p(d) \sigma_Y \bar{\varepsilon}^p + g^h(d) \frac{1}{2} h \bar{\varepsilon}^{p2}. \quad (21)$$

See [hyperelasticity.pdf](#) for other hyperelastic potentials with tension-compression asymmetry.  
 See [plasticity.pdf](#) for a detailed derivation.

Balance laws and constitutive equations:

$$\nabla \cdot \mathbf{P} + \rho_0 \mathbf{B} = \mathbf{0}, \quad (22)$$

$$-\nabla \cdot \boldsymbol{\pi}, \nabla d + \boldsymbol{\pi}, \dot{d} \geq 0, \quad \dot{d} \geq 0, \quad (23)$$

$$\rho_0 r - \pi, \bar{\varepsilon}^p \dot{\bar{\varepsilon}}^p - \pi, d \dot{d} = \rho_0 c \dot{T}, \quad (24)$$

The constitutive relation between the Kirchhoff stress and the deformation gradient is

$$\boldsymbol{\tau} = \mathbf{g}^e(\mathbf{d}) \boldsymbol{\tau}^{(A)} + \boldsymbol{\tau}^{(I)}, \quad (25a)$$

$$\boldsymbol{\tau}^{(A)} = \frac{1}{2} H(J-1) K_s (J^2 - 1) \mathbf{I} + \mu_s \operatorname{dev}(\mathbf{b}^e), \quad (25b)$$

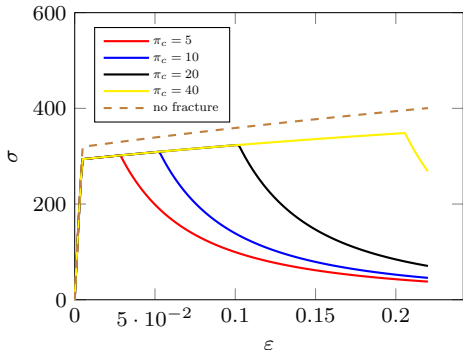
$$\boldsymbol{\tau}^{(I)} = \frac{1}{2} H(1-J) K_s (J^2 - 1) \mathbf{I}. \quad (25c)$$

The Kuhn-Tucker loading/unloading conditions are

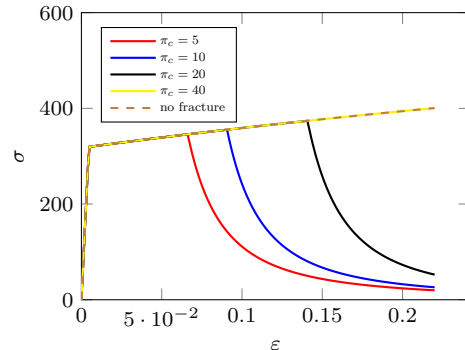
$$\phi(\mathbf{N}^p, \bar{\varepsilon}^p, d) = \|\operatorname{dev}(\boldsymbol{\tau})\| - \sqrt{\frac{2}{3}} \left[ \mathbf{g}^p(\mathbf{d}) \sigma_Y + \mathbf{g}^h(\mathbf{d}) h \bar{\varepsilon}^p \right] \leq 0, \quad \dot{\bar{\varepsilon}}^p \geq 0, \quad \dot{\bar{\varepsilon}}^p \phi(\mathbf{N}^p, \bar{\varepsilon}^p, d) = 0, \quad (26)$$

and the flow rule is

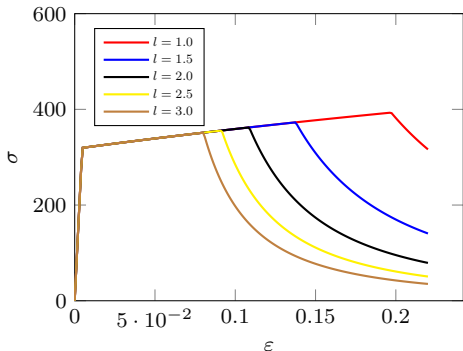
$$\dot{\mathbf{F}}^p \mathbf{F}^{p-1} = \dot{\bar{\varepsilon}}^p \mathbf{N}^p, \quad \mathbf{N}^p = \sqrt{\frac{3}{2}} \frac{\operatorname{dev}(\boldsymbol{\tau})}{\|\operatorname{dev}(\boldsymbol{\tau})\|}, \quad \det(\mathbf{F}^p) = 1. \quad (27)$$

Unperturbed elastic-plastic behavior

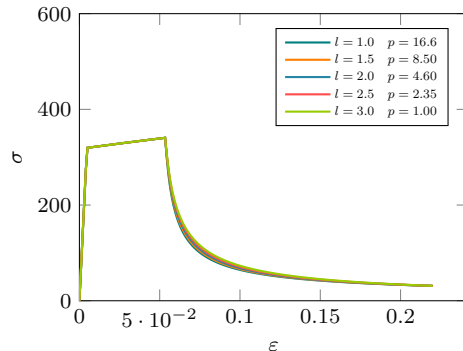
(a)



(b)

Regularization length-insensitive fracture strength

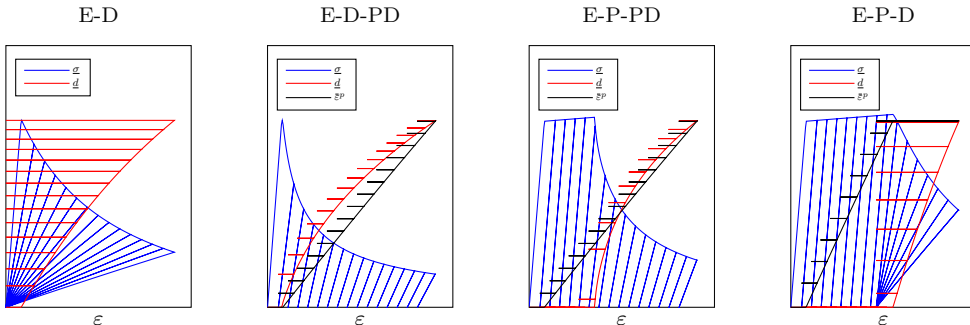
(a)



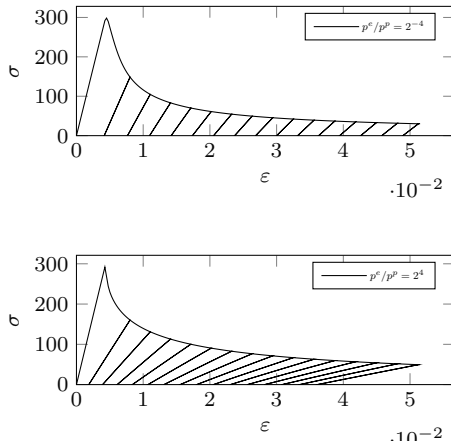
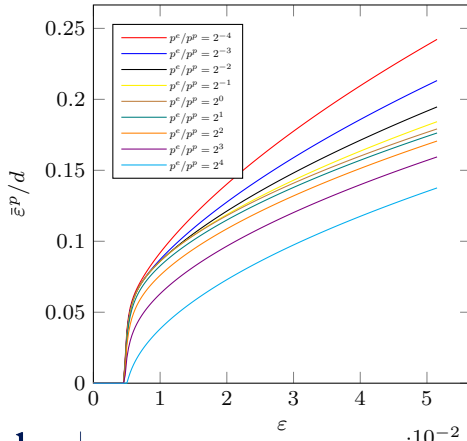
(b)

Following Alessi et. al. there are four representative stages.

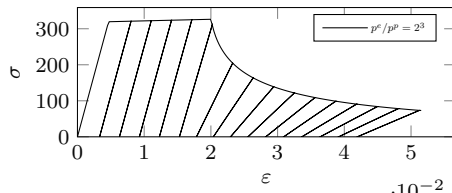
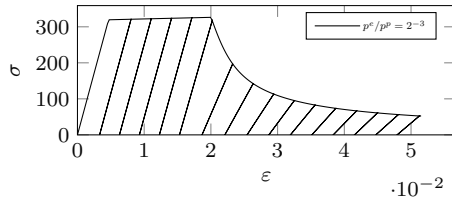
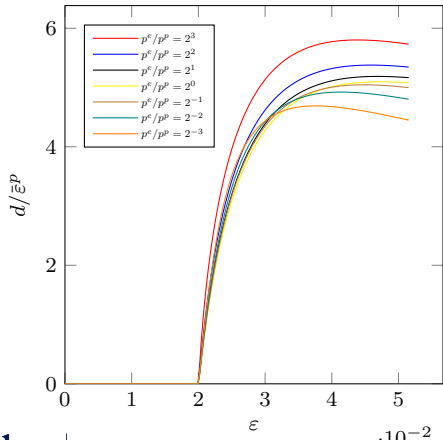
- ▶ E: elastic loading
- ▶ D: damage softening
- ▶ P: plastic hardening
- ▶ PD: mix of plastic hardening and damage softening



The shapes of the degradation functions (in particular, their derivatives) determine the amount of plastic dissipation during the damage softening process. **The E-D process may be viewed as a limiting case of the E-D-PD process.** Similarly, the E-P-D process may be viewed as a limiting case of the E-P-PD process.



The shapes of the degradation functions (in particular, their derivatives) determine the amount of plastic dissipation during the damage softening process. The E-D process may be viewed as a limiting case of the E-D-PD process. Similarly, the E-P-D process may be viewed as a limiting case of the E-P-PD process.



Dugdale's model and Barenblatt's model lead to different crack paths in a three-point bending problem.

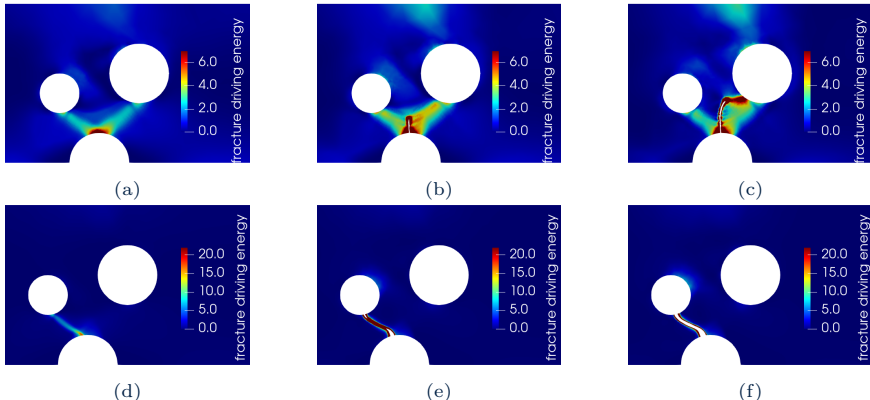


Figure: Contour plots of the total fracture driving energy  $\pi_{\text{elastic}}^{(A)} + \pi_{\text{plastic}}$  for (a-c) Dugdale's cohesive model and (d-f) Barenblatt's cohesive model.

For the Committee

Courses taken

Courses TA'd

RCR trainings

Past work

Theory

Soil Desiccation

Intergranular Fracture in UO<sub>2</sub>

Future work

Proposal

Timeline

**Preliminary results and findings**

Towards ductile fracture

Incorporating thermal effects

References

**Neumann-type boundary conditions** can be defined based on an approximated crack surface normal:

$$\int_{\partial\Omega} \mathbf{t} \, dA \approx \int_{\Omega_t} \mathbf{t} \|\nabla_{\mathbf{x}} d\| \, dV = \int_{\Omega_0} \mathbf{T} \|\nabla d\| \, dV, \quad (28)$$

where  $\mathbf{t}$  is some surface flux and  $\mathbf{T} = \mathbf{F}^{-1} \cdot \mathbf{t}$  is its material form.

$\Gamma$ -convergence of this approximation has been sketched in [21]. A numerical investigation of the  $\Gamma$ -convergence can be found in [22] in the context of finite cell method.

[13] provides a similar approximation based on finite-differencing arguments.

Many studies on pressurized crack and hydraulic fracture have used a special case of the approximation where  $\mathbf{t} = p_0 \tilde{\mathbf{n}}$  with  $p_0$  being a scalar-valued pressure field.

See `neumann.pdf` for an example of the approximated Neumann BC.

### A better approximation of the crack surface normal

The closed-form solution to the phase-field in 1D, depending on the specific choice of the local fracture dissipation function, is

$$d(\tau; l) = \begin{cases} \left(1 - \frac{\tau}{2l}\right)^2, & w(d) = w_l(d), \\ 1 - \exp(-\tau/l), & w(d) = w_q(d), \end{cases} \quad (29)$$

A Cahn-Hilliard approximation to the crack surface density takes the form

$$\gamma_4(d; l) = \frac{1}{c_0 l} [w(d) + 2l^2 \nabla d \cdot \nabla d + l^4 (\Delta d)^2], \quad (30)$$

and a  $C^\infty$  closed-form solution exists when  $w(d) = w_q(d)$ , i.e.

$$d(\tau; l) = \exp(-\tau/l) \left(1 + \frac{\tau}{l}\right), \quad (31)$$

and the approximation of the crack surface normal will be smooth almost everywhere.

### Thermal effects

Disregarding the adiabatic assumption and taking into account the aforementioned approximation to heat flux, the modified heat equation can be written as

$$g(d)\rho_0 c \dot{T} = g(d)\rho_0 r - g(d)\nabla \cdot \kappa \nabla T - \pi_{,\bar{\varepsilon}^p} \bar{\varepsilon}^p - \pi_{,d} d, \quad (32)$$

Thermal-elastic coupling can be introduced by an inelastic potential  $r(T; T_0, \alpha) \text{tr}(\boldsymbol{\varepsilon})$  where  $T_0$  is the reference temperature and  $\alpha$  is the thermal expansion coefficient.

Heat generation due to plasticity has been considered in the heat equation. Thermal softening in the plastic regime can be defined by the degradation of hardening modulus as a function of temperature  $h = \tilde{h}(T)$ .

-  Mingyi Hong and Zhi-Quan Luo.  
On the linear convergence of the alternating direction method of multipliers.  
*Mathematical Programming*, 162(1-2):165–199, 2017.
-  N. Moelans, B. Blanpain, and P. Wollants.  
Quantitative analysis of grain boundary properties in a generalized phase field model for grain growth in anisotropic systems.  
*Phys. Rev. B*, 78:024113, Jul 2008.
-  G.A. Francfort and J.J. Marigo.  
Revisiting brittle fracture as an energy minimization problem.  
*Journal of the Mechanics and Physics of Solids*, 46(8):1319–1342, 1998.
-  B. Bourdin, G.A. Francfort, and J.J. Marigo.  
Numerical experiments in revisited brittle fracture.  
*Journal of the Mechanics and Physics of Solids*, 48(4):797–826, 2000.

-  Blaise Bourdin, Gilles A Francfort, and Jean-Jacques Marigo.  
The variational approach to fracture.  
*Journal of elasticity*, 91(1-3):5–148, 2008.
-  A. Karma, D. A. Kessler, and H. Levine.  
Phase-field model of mode III dynamic fracture.  
*Physical Review Letters*, 87(4):045501–1–4, 2001.
-  A. Karma and A. E. Lobkovsky.  
Unsteady crack motion and branching in a phase-field model of brittle fracture.  
*Physical Review Letters*, 93(10):245510, 2004.
-  H. Henry and H. Levine.  
Dynamic instabilities of fracture under biaxial strain using a phase field model.  
*Physical Review Letters*, 93(10):105504, 2004.
-  R. Spatschek, C. M. Gugenberger, and E. Brener.  
Phase field modeling of fracture and stress-induced phase transitions.  
*Physical Review E*, 75:066111, 2007.

-  H. Amor, J. J. Marigo, and C. Maurini.  
Regularized formulation of the variational brittle fracture with unilateral contact: Numerical experiments.  
*Journal of the Mechanics and Physics of Solids*, 57(8):1209–1229, 2009.
-  Michael Johns Borden.  
*Isogeometric analysis of phase-field models for dynamic brittle and ductile fracture.*  
PhD thesis, The University of Texas at Austin, 2012.
-  Xiaoxuan Zhang, Andreas Krischok, and Christian Linder.  
A variational framework to model diffusion induced large plastic deformation and phase field fracture during initial two-phase lithiation of silicon electrodes.  
*Computer Methods in Applied Mechanics and Engineering*, 312:51–77, 2016.
-  Christian Miehe, Lisa-Marie Schaenzel, and Heike Ulmer.  
Phase field modeling of fracture in multi-physics problems. part i. balance of crack surface and failure criteria for brittle crack propagation in thermo-elastic solids.  
*Computer Methods in Applied Mechanics and Engineering*, 294:449–485, 2015.

-  Heike Ulmer, Martina Hofacker, and Christian Miehe.  
Phase field modeling of brittle and ductile fracture.  
*PAMM*, 13(1):533–536, 2013.
-  Roberto Alessi, Jean-Jacques Marigo, Corrado Maurini, and Stefano Vidoli.  
Coupling damage and plasticity for a phase-field regularisation of brittle, cohesive and ductile fracture: one-dimensional examples.  
*International Journal of Mechanical Sciences*, 149:559–576, 2018.
-  Marreddy Ambati, Roland Kruse, and Laura De Lorenzis.  
A phase-field model for ductile fracture at finite strains and its experimental verification.  
*Computational Mechanics*, 57(1):149–167, 2016.
-  Michael J Borden, Thomas JR Hughes, Chad M Landis, Amin Anvari, and Isaac J Lee.  
A phase-field formulation for fracture in ductile materials: Finite deformation balance law derivation, plastic degradation, and stress triaxiality effects.  
*Computer Methods in Applied Mechanics and Engineering*, 312:130–166, 2016.

-  Fernando P Duda, Angel Ciarbonetti, Pablo J Sánchez, and Alfredo E Huespe.  
A phase-field/gradient damage model for brittle fracture in elastic–plastic solids.  
*International Journal of Plasticity*, 65:269–296, 2015.
-  Charlotte Kuhn, Timo Noll, and Ralf Müller.  
On phase field modeling of ductile fracture.  
*GAMM-Mitteilungen*, 39(1):35–54, 2016.
-  C Miehe, S Teichtmeister, and F Aldakheel.  
Phase-field modelling of ductile fracture: a variational gradient-extended plasticity-damage theory and its micromorphic regularization.  
*Philosophical Transactions of the Royal Society A: Mathematical, Physical and Engineering Sciences*, 374(2066):20150170, 2016.
-  Chukwudi Chukwudzie, Blaise Bourdin, and Keita Yoshioka.  
A variational phase-field model for hydraulic fracturing in porous media.  
*Computer Methods in Applied Mechanics and Engineering*, 347:957–982, 2019.

-  Lam Nguyen, Stein Stoter, Thomas Baum, Jan Kirschke, Martin Ruess, Zohar Yosibash, and Dominik Schillinger.  
Phase-field boundary conditions for the voxel finite cell method: Surface-free stress analysis of ct-based bone structures.  
*International journal for numerical methods in biomedical engineering*, 33(12):e2880, 2017.